Sensors & Actuators: B. Chemical 333 (2021) 129453

Contents lists available at ScienceDirect

Sensors and Actuators: B. Chemical

journal homepage: www.elsevier.com/locate/snb

# Self-organized plasmonic metasurfaces: The role of the Purcell effect in metal-enhanced chemiluminescence (MEC)

Daler R. Dadadzhanov [a,b], Igor A. Gladskikh [b], Mikhail A. Baranov [b], Tigran A. Vartanyan [b], Alina Karabchevsky [a,*]

[a] School of Electrical and Computer Engineering, Ben-Gurion University of the Negev, Beer-Sheva 8410501, Israel
[b] ITMO University, 49 Kronverksky Ave., 197101 St. Petersburg, Russia

ARTICLE INFO

*Keywords:*
Plasmonic nanoparticles
Chemiluminescence
Microfluidic chip
Label-free sensor
Metal-enhanced chemiluminescence
Luminol

ABSTRACT

Chemiluminophores are entities, which exhibit wide-band light emission without any external light source, just caused by a chemical reaction. Since chemiluminescence usually yields to unfavorable competition with other channels of chemical energy dissipation, plasmonic nanoparticles can be employed to enhance the chemiluminescence quantum yield via acceleration of the radiative decay rate due to the Purcell effect. On the other hand, the catalytic action of metallic surface can contribute to the chemical reaction rate. Both mechanisms can lead to substantial chemiluminescence intensity enhancement when chemiluminophores are in contact with metal nanoparticles. Although the investigations devoted to MEC are numerous, the relative roles of the Purcell effect and catalysis in the chemiluminescence enhancement are still unclear. In this paper, with the use of a thin inert spacer layer deposited on top of a silver metasurface, we observe a moderate decrease of the chemiluminescence enhancement, which favors an electrodynamic mechanism. We also check that the continuous silver film without plasmon resonances causes no measurable chemiluminescence enhancement. As the results supported the electrodynamic mechanism of MEC, silver nanoparticles with suitable properties have been fabricated via physical vapor deposition on the substrate. We have theoretically optimized the silver nanoparticles shape and size distributions to tune their localized surface plasmon bands for the best overlap with the emission of luminol and some other chemiluminophores. Our design for plasmonic nanoparticles placed on the dielectric material may motivate a new generation of chemiluminescence-based devices for sensing applications.

## 1. Introduction

Chemiluminescence, or a "liquid light" effect, is an emission of photons resulting in an exothermic chemical reaction [1]. This effect is applied in various fields from forensic science [2] to industrial bio-chemistry [3,4]. Luminol, a widely used chemical that exhibits chemiluminescence, generates blue light under certain conditions [5]. Forensic investigators use luminol to detect blood traces amounts at crime scenes as the chemical reaction can be catalyzed by the iron contained in hemoglobin. Biologists use luminol in cellular assays to detect copper, iron, and specific proteins [6]. However, the intensity of luminol chemiluminescence is quite low, significantly limiting its potential applications. Particularly, the quantum efficiency of the chemiluminescence process is low due to the competition with a multitude of non-radiative decay processes [7]. Hence, radiative decay acceleration of the chemiluminophore excited state is a reliable way to enhance the chemiluminescence yield that attracts the attention of many scientists [1,8,9]. In turn, the surface plasmon resonance in metallic nanoparticles [10,11] can be employed for the acceleration of these radiative transitions.

The schematics of the chemiluminescence enhancement mechanism is summarized in Fig. 1. The luminol excitation in the course of a chemical reaction with an oxidizer followed by two competitive decay routes: radiative and non-radiative (Fig. 1a). The effect of plasmon nanoparticles on the luminol emission is depicted in Fig. 1b. The expected chemiluminescence enhancement originates due to the Purcell effect that couples the luminol emission with the enhanced local fields in the vicinity of the plasmon nanoparticle [12]. As a result, the density of photon states increases, and the process of chemiluminescence is boosted. This effect reaches its maximum in the close proximity of the nanoparticles and vanishes at larger distances. At the same time, direct contact with the metal surface is known to cause luminescence

* Corresponding author.
*E-mail addresses:* daler.dadadzhanov@gmail.com (D.R. Dadadzhanov), alinak@bgu.ac.il (A. Karabchevsky).

https://doi.org/10.1016/j.snb.2021.129453
Received 24 July 2020; Received in revised form 17 December 2020; Accepted 3 January 2021
Available online 30 January 2021

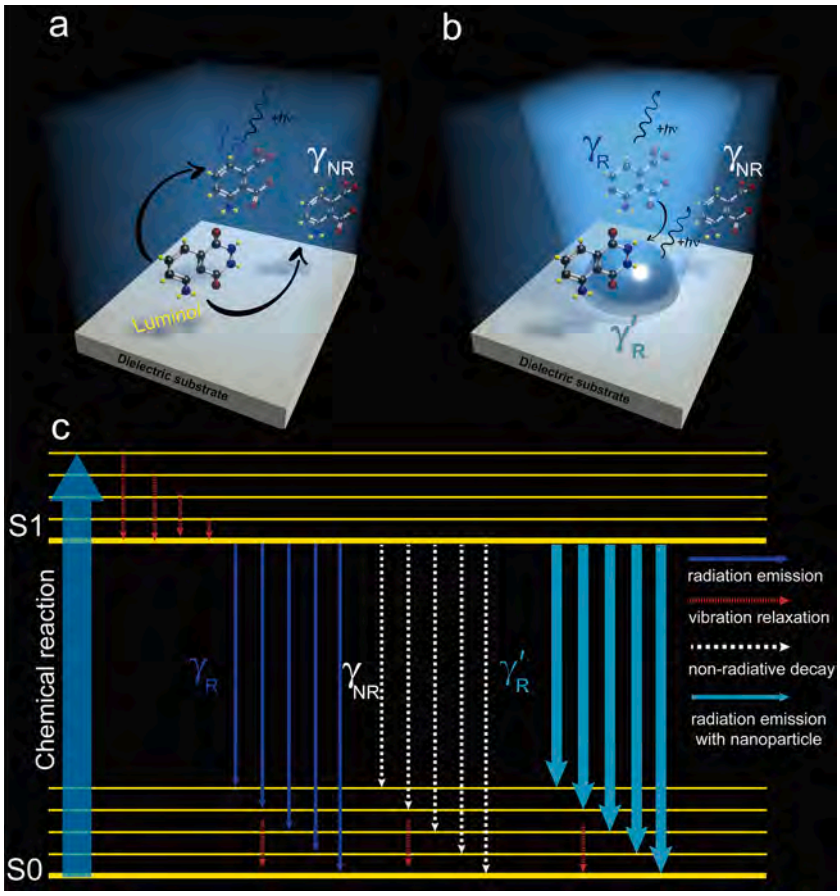


**Fig. 1.** Schematic enhancement mechanism of the chemiluminescence effect. (a) The luminol oxidation leads to competitive processes of radiative decay (emission of a photon) and non-radiative decay (production of heat). The blue color emission is attributed to the luminol emission. (b) The proposed mechanism of the metal-enhanced chemiluminescence in the presence of AgNP. (c) The general Jablonski energy level diagram modified for the chemiluminescence emission in the presence of AgNP [53]. The chemiluminescence emission origin as a result of chemical oxidation process. The molecular transition from the excited (*S1*) to the electron ground state (*S0*) leads to the photon emission and heat production. $\gamma_R$ and $\gamma_{NR}$ are the radiative and non-radiative decay rates of the luminol molecules. $\gamma_{R'}$ is the radiative decay rate of luminol molecules in the vicinity of AgNP. (For interpretation of the references to color in this figure legend, the reader is referred to the web version of this article.)

quenching. The luminescence quantum yield ($\eta$) is determined by the competition of radiative ($\gamma_R$) and non-radiative ($\gamma_{NR}$) decay processes. When $\gamma_{NR}$ is larger or on the same order of magnitude as $\gamma_R$, the growth of $\gamma_R$ leads to the substantial growth of the luminescence quantum yield, provided that the growth of $\gamma_{NR}$ is smaller than the growth of $\gamma_R$. Therefore, the chemiluminescence quantum yield in the presence of metal nanoparticles grows according to the formula $\eta \propto \frac{\gamma_R'}{\gamma_R + \gamma_{NR}'}$, where $\gamma_R'$ and $\gamma_{NR}'$ are the modified radiative and non-radiative decay with the presence of metal nanoparticles. Indeed, this phenomenon known as metal-enhanced fluorescence (MEF) was reported in previous research [13,14]. Compared to MEF, where the molecule initially has to be pumped by an external light source, metal-enhanced chemiluminescence (MEC) stems from the chemical oxidation process [15,16], as shown in the Jablonski diagram (Fig. 1c). Thus, the chemiluminescence intensity can be boosted by plasmon nanoparticles provided the condition of the increased radiative decay rate ($\gamma_R' > \gamma_R$) is fulfilled while $\gamma_{NR}$ does not substantially grow.

To maximize the chemiluminophores-nanoparticles pair interaction, two conditions should be satisfied: (1) the plasmon absorption band and the chemiluminescence emission band have to possess a resonant overlap [17,18] and (2) the chemiluminophore molecules have to be placed in close proximity with metal nanoparticles [1,19]. In this case, the shape and material of the particles have to be accurately chosen to ensure the overlapping of their absorption plasmonic band with the emission band of the chemiluminophores [18]. In our previous work, the new proof-of-concept experiment was performed with a microfluidic chip [1], wherein we utilized the commercially available nanoparticles with the non-optimized spectral location of the absorption plasmon absorption band. Therefore, the chemiluminescence quantum yield can be further improved with specially designed surfaces.

The microfluidic chip can be applied as an experimental tool for observing the chemiluminescence effect. Such chips are employed to study low volume samples by isolating key phenomena from the surrounding environment [20]. The flow-injection in microfluidic chips helps obtain the efficient chemical reaction when the chemiluminophores and their oxidants are mixed to emit light. Advanced developments in the field of microfluidic technology platforms have already led to the creation of high-demanded applications such as the lung-on-a-chip platform [21–23], single-cell functional proteomics [24,25]. Moreover, these developments allow measuring the dynamics of green fluorescence protein [26,27]. The efficient emission of luminol is expected to be implemented in forensic science-on-a-chip and accurate DNA profiling with active lasing dust.

In this paper, we report on the novel metal-enhanced chemiluminescence (MEC) sensor, which has significantly improved MEC-substrate with resistance to organic solvents and mechanical damage required for microfluidic systems. The goal of this study is to explore the opportunities of chemiluminescent enhancement provided by the planar ensembles of plasmonic metal nanoparticles. We show that the self-organized metasurfaces with broadband and tunable plasmon resonances, which are necessary for the effective interaction between nanoparticle acceptors and chemiluminophore donors, may be obtained via previously developed manufacturing technology [28–30]. Moreover, we demonstrate the benefits of fabricating silver nanoparticles (AgNPs) on a dielectric substrate using physical vapor deposition (PVD). We have found that the spectral plasmon band position of AgNPs is tuned via the PVD process and subsequent annealing treatment. The spectral position of the plasmon absorption band may be controlled by the amount of the sputtered metal in order to provide a spectral overlap with the emission bands of chemiluminescent species. Consequently, the fulfillment of the requirements for effective acceleration of radiative transitions in

**Table 1**
An overview of chemiluminescence sensors using different enhancement strategies.

| Chemiluminescent system | Comments | Reference |
|---|---|---|
| Ag and Au with luminol-NaOH | The CL enhancement in microfluidic chip initiated by small sphere nanoparticles. The enhancement factor is up to 4-fold. | [1] |
| Ag-luminol-$H_2O_2$-HRP | A silver modified immunoassay for determination mycotoxins using luminol with amplified chemiluminescence on the chip through the localized surface plasmon resonance phenomenon. The enhancement factor is ~ 2-fold. | [34] |
| Cr, Cu, Ni, and Zn metal films with green dye | The chemiluminescence intensity from chemiluminophore (commercially available kits, Omnioglow company – acridan oxalate system) was enhanced by metal films. The enhancement factor is up to 3-fold. | [31] |
| Al, Au, Ag metal films with red, green and blue dyes | The luminophores dyes excited the surface plasmons on thin continuous metal films without incident excitation light. The CL species/SPR coupling demonstrates a highly polarized and directional emission. The enhancement factor was not estimated. | [33] |
| Ag SIF with green dye-$H_2O_2$ | The commercially available chemiluminophores from glowstick (commercially available kits, Omnioglow company) was enhanced by metal films. The enhanced chemiluminescence intensity is around 20-fold. | [32] |

luminol seems feasible.

Previously, all attempts to enhance the weak chemiluminescence of luminol by plasmonic nanoparticles revealed no sufficient information on the enhancement mechanisms either catalysis or the effect of an enhanced near-field of nanoparticles. According to [4], both the purely chemical catalytic effect of the contact with the metal surface and the Purcell electromagnetic effect contribute to the MEC activity, but the relative role played by the two in the observed enhancement is not clearly determined. Table 1 represents a brief overview of the latest results related to the chemiluminescent enhancements of luminol as well as chemiluminescent species used in glow sticks [31–33]. The essential peculiarity of luminol is its biocompatibility, which in turn allows its use for pharmaceuticals and biological sciences. Based on our recent work [1] using the colloidal solution of metal nanospheres with luminol flowing in a microfluidic chip, we have switched from large consumable volumes of nanoparticles to small ones by using a planar metasurface of silver nanoparticles. To the best of our knowledge, this is the first application of the plasmon metasurfaces fabricated on a dielectric substrate for luminol chemiluminescence enhancement. Our experimental results provide clear evidence that the catalytic action of silver is of minor importance as compared to the Purcell effect. In this regard, the metal metasurface optimization, which allows for chemiluminescence intensity enhancement by means of the electromagnetic effects is of particular importance. Numerical simulations were used to put the obtained experimental results in a bigger picture of opportunities connected with a range of chemiluminescent agents and substrates for silver deposition, particularly. Owing to the calculated results it makes it possible to choose the experimentally realizable shape of metal nanoparticles that ensures the perfect overlap between the plasmon bands of metal metasurface and chemiluminescent bands of chemiluminophores.

## 2. Materials and methods

### 2.1. Synthesis of supported silver nanoparticles via physical vapor deposition

We fabricated AgNPs on a microscope glass slide using the physical vapor deposition in a vacuum chamber PVD-75 (Kurt J. Lesker). All microscope slides were preliminarily washed in ethanol and then washed with distilled water. AgNP ensemble was grown according to the Volmer-Weber mechanism [35]. The equivalent thickness of the silver film was controlled by a quartz crystal microbalance during the growth and was 5 nm. The silver plate (99.99% purity) was evaporated in high vacuum ($1{\cdot}10^{-6}$ Torr). Then, the obtained silver film was annealed at 200 °C. The spectral position of the plasmon absorption band was controlled by the amount of the evaporated metal and the evaporation rate as well as by the temperature and the duration of the subsequent annealing [28,36]. To obtain the ensemble of AgNPs, the silver deposition was used at a rate of 0.1 Åper second. The blue-shift of the plasmon resonance band with a maximum around 482 nm was achieved by thermal annealing of the silver film for 30 min. To provide better adhesion of AgNPs to the substrate and ensure their stability in the oxidizing environment in the course of the chemiluminescence studies, the laser-assisted approach was applied. The laser exposure was realized by the third harmonic (355 nm) of a Q-switched Nd:YAG laser (SOLAR Laser Systems). The pulse duration and the repetition rate were 10 ns and 10 Hz, respectively. The laser beam, with the diameter of 8 mm, was focused on the AgNP ensemble supported on the glass substrate and exposured through the perforated paper mask. The fluence was controlled by optical filters and varied from 50 mJ/cm$^2$ to 100 mJ/cm$^2$. The stronger adhesion of silver nanoparticles to the substrate was achieved by laser irradiation with 1000 pulses (see Supplementary file, Figure S1). The AgNP substrate covered with 2 nm $SiO_2$ layer was prepared to estimate the role of the catalysis effect from silver according to the procedure in Ref. [37].

### 2.2. Characterization studies

Scanning electron microscope images of the supported silver nanoparticles were obtained with MERLIN (Carl Zeiss) microscope at 15 kV. Optical extinction spectra of silver nanoparticles on the substrate were collected using an SF-56 spectrophotometer (LOMO) with 1 nm resolution in the range of 250–1100 nm at room temperature. The chemiluminescent spectra of luminol were recorded by a charge-coupled device (CCD), Lumenera Infinity 2-3C (Lumenera Corporation, 7 Capella Crt. Ottawa, Ontario, Canada). A digital photographic camera (Canon 70D) with a high integration time was used to capture chemiluminescence light and record the images of glowing samples. In addition to the experiments with luminol, the chemiluminescent spectra of 9,10-diphenylanthracene (DPA) molecules were also obtained by a spectrofluorometer (Cary Eclipse) while the excitation source of the spectrofluorometer was off.

### 2.3. Complexes of AgNP@Chemiluminophore

A stock solution (*next denoted as "solution 1"*) of 3-aminophthalhydrazide (luminol) with the concentration of $2.8{\cdot}10^{-5}$ M in deionized water, purchased from Sigma Aldrich, was mixed with sodium hydroxide (NaOH), with the concentration of 1 mM. A 5% solution of sodium hypochlorite (NaOCl), was used as an oxidizing agent (*next denoted as "solution 2"*). Chemiluminescent radiation occurs as a result of a chemical reaction between organic chemiluminophore molecules and an oxidizing agent. In addition, we conducted an experiment with DPA. All chemiluminophore species were placed between two microscope glass slides, one of which was partially covered with silver nanoparticles embedded in advance.

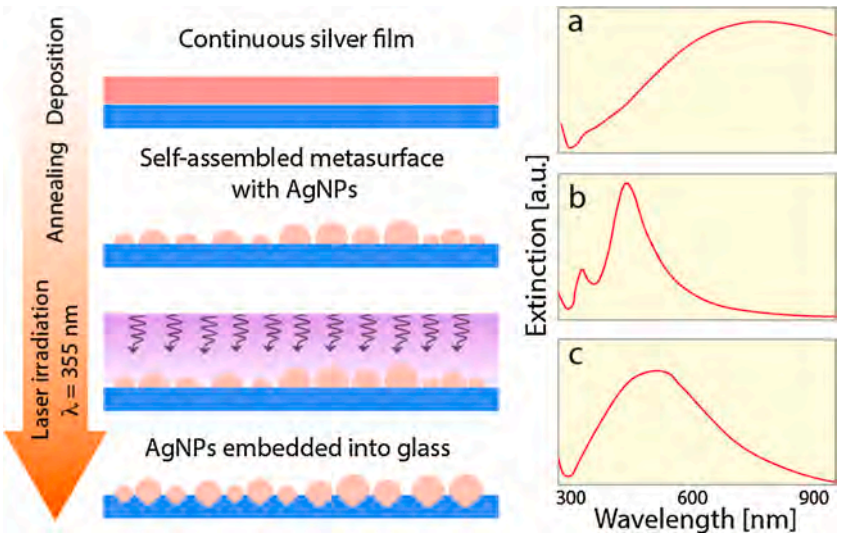


**Fig. 2.** The proposed process scheme of silver nanoparticles ensemble preparation and the extinction spectra evolution: (a) a continuous film, (b) after annealing at 200 °C, and (c) after laser irradiation.

### 2.4. Numerical simulation

The Finite-Element-Method (FEM) implemented in COMSOL Multiphysics 5.4 software (Wave Optics Module) was used to solve Maxwell's equations for stationary problems. We calculated absorption, scattering and extinction cross-section spectra of AgNPs varying their shapes and substrates to predict the behavior in combination with chemiluminophores. We have built a 3D box that contains two domains, with a width of 200 nm, intended for the dielectric substrate and surrounding media. A perfectly matched layer (PML) was included as a physical domain with the thickness of 150 nm to absorb scattered light. We define the thickness of PML as a half of the incident wavelength. The PML layer was divided by 8 equidistant layers. The silver nanoparticle was placed in the center domain with subsequent meshing in the form of tetrahedral elements. Maximum element size of the surrounding medium, dielectric substrate and nanoparticle were chosen as $\lambda/6$ when the electromagnetic incident field oscillated parallel to the substrate with a $k$-vector perpendicular to the substrate. The parametric sweep was used to calculate the absorption, scattering and extinction cross-sections of plasmonic nanoparticles as described in Ref. [38], in the range of 350–750 nm. Since the dephasing time of plasmon silver nanoparticles (for $r > 10$ nm) deposited on a dielectric substrate remained practically unchanged as shown in [39], the correction for a quantum-confinement size effect was neglected. Thus, the complex refractive index of the AgNP from the experimental work of Johnson and Christy for bulk silver [40] was implemented for the modeling.

## 3. Results and discussion

### 3.1. Experimental results

In this section, we experimentally investigate the relative contributions of plasmonic and catalytic mechanisms in the chemiluminescence intensity enhancement due to the silver metasurface. Firstly, we consider the process scheme of step-by-step morphology modification starting from a deposited thin film to the inhomogeneous ensemble of silver nanoparticles, as shown in Fig. 2. This technique was used to obtain plasmonic nanoparticles optimized for the luminol chemiluminescence enhancement. Chemiluminescence of different chemiluminophores may be enhanced via the suggested technique, the dedicated choices of substrates, and annealing procedures [28]. In the previous work [29] we showed that an increase of the annealing time for AgNPs, from 0 to 60 min with the temperature of 190 °C, leads to a narrowing and blue-shift of the extinction spectrum, which indicates a decrease in the size distribution of silver nanoparticles. It was also shown that at low annealing temperatures of 70 °C, the extinction spectra are broader. Nevertheless, it was demonstrated that upon subsequent annealing, the nanoparticles took the form of spheroids.

Fig. 2a illustrates the extinction spectrum of the deposited continuous silver film, whose plasmon absorption band is out of the spectral

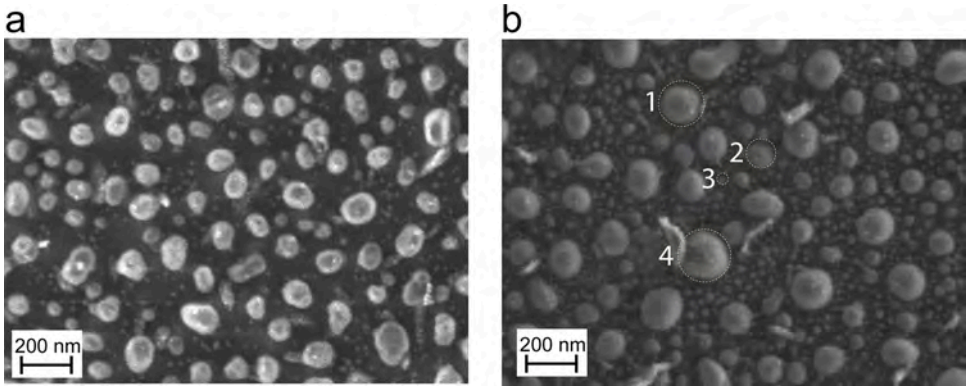


**Fig. 3.** Scanning electron microscope images of AgNPs on the glass substrate. The scale bar is 200 nm. The size distribution of AgNPs before (a) and after laser irradiation (b). AgNPs in (b) varying from 10 to 200 nm (1–155 nm, 2–105 nm, 3–20 nm, 4–200 nm).

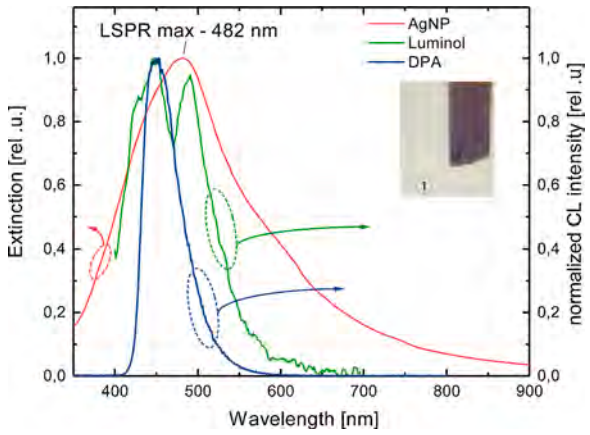


**Fig. 4.** The extinction spectra overlap of AgNPs obtained via PVD with subsequent thermal annealing/laser exposure (red curve) with the chemiluminescence (CL) emission spectra of: luminol (green curve) and DPA (blue curve). The inset shows a photograph of (1) the cover-glass partially covered with (2) AgNPs. All spectra are normalized. The arrows on the curves point towards of the corresponding axis. (For interpretation of the references to color in this figure legend, the reader is referred to the web version of this article.)

region necessary to overlap with the luminol emission band. Then, using the time/temperature dependence of the annealing process, we achieve the desired shape and size distributions of AgNPs that lead to the plasmonic band in the aimed spectral range. However, the fabricated self-organized metasurfaces of AgNPs were mechanically unstable and may be damaged by organic/non-organic solvents, for instance, water, ethanol, hexane. To overcome this limitation, we developed a novel approach for strong adhesion of AgNPs to the dielectric substrates. In particular, after annealing process, the thin silver film was exposed to the pulsed laser irradiation at the wavelength of 355 nm. As it is seen in Fig. 2b, the extinction spectrum after the subsequent annealing process is characterized by the sharp absorption plasmon resonance band in the visible range. Under the laser irradiation, the plasmon band broadens whereas its overlap with the chemiluminescence emission spectra of luminol becomes greater (Fig. 2c). From the experimental point of view, it is essential to improve the chemical and mechanical stability of the metal films because the chemical reagents used in the chemiluminophore solution are very aggressive. We found that rinsing with "*solution 1*" and ethanol does not degrade the laser-irradiated substrate with the AgNP metasurface. This is confirmed by the stability of the optical absorption spectra in Figure S1 for sample 2. It is worth noting that the adhesion of AgNPs to the substrate also improved (Fig. 2c), and this property was confirmed by scratching the film with a sharp object (see Table S1 and S2). Thus, laser irradiation leads to the formation of samples that are resistant to organic solvents and resistant to mechanical damage. These samples are suitable for chemiluminescence experiments as opposed to untreated samples.

To clarify the morphology of the prepared AgNP metasurface, we analyzed the SEM images before and after the annealing process as depicted in Fig. 3. We observe two distinct ensembles of larger and smaller nanoparticles in both images. The image of AgNPs obtained after annealing procedure shows the presence of rather similar larger nanoparticles with diameters not exceeding 160 nm. After the laser irradiation, all AgNPs becomes larger and more rounded. At the same time, the size distribution becomes broader and the distinction between ensembles of larger and smaller particles becomes more pronounced (see Fig. 3). Consequently, the extinction spectrum of the silver nanoparticles shifts and broadens, as seen in Fig. 2c.

The measured extinction spectra of the AgNP metasurface after the laser irradiation exhibit the pronounced plasmon bands in range of 350 to 650 nm with a maximum at 482 nm (Fig. 4). The inset of Fig. 4 shows an image of the substrate (1) and the substrate with the AgNPs (2) fabricated via PVD and subjected to both the subsequent annealing and laser irradiation. We noticed that the film has a definite brown color that corresponds to the spectral position of the absorption band of the fabricated AgNPs, as shown in Fig. 4. As it was mentioned above, to boost the chemiluminescent emission, the overlap between the chemiluminophore (donor) luminescent band and AgNPs (acceptor) absorption band is required. To show this overlap, the normalized chemiluminescent spectrum (CL) of luminol is plotted in the same graph. The chemiluminescent spectra of luminol consists of two overlapping emission bands with maxima at the wavelengths of 452 nm and at the wavelengths of 489 nm, respectively. The plasmon band of the prepared AgNP samples is overlapped with both luminol chemiluminescence emission bands. In addition, we observed that the DPA chemiluminescent emission band (Fig. 4) spectrally is also overlapped with the absorption peak of plasmon band.

Finally, the enhanced near-field effect of synthesized AgNPs on chemiluminophore molecules has been investigated. We employed a straightforward, experimental procedure in order to show the MEC effect presence. We dripped 30 µl of "*solution 1*" onto the bare glass

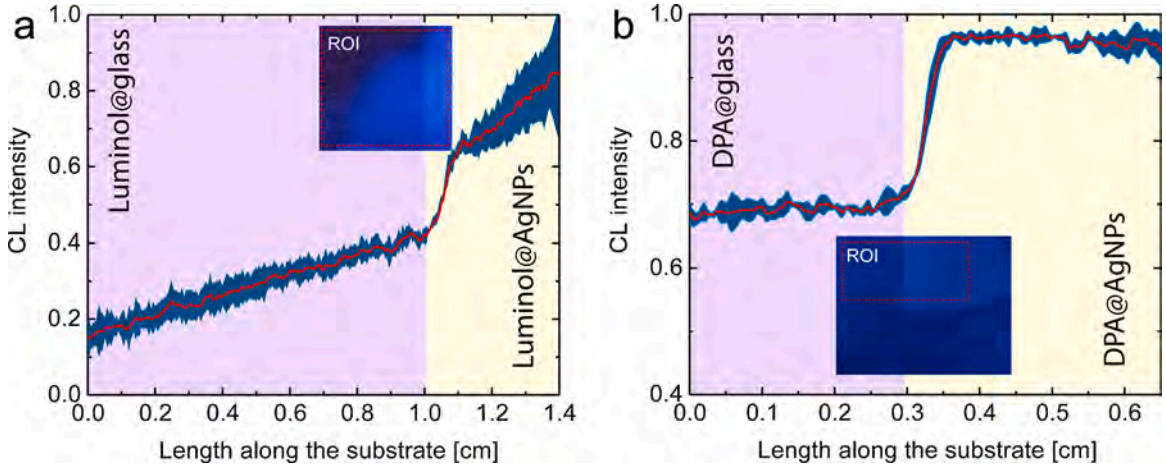


**Fig. 5.** Distribution of chemiluminescence intensities over the indicated regions of interest (ROI): (a) luminol and (b) DPA. Red curves represent the chemiluminescence intensity integrated over the vertical axes and plotted against the horizontal axes of the corresponding chemiluminescent images. The jumps at the borders of dedicated silver metasurfaces are clearly seen both in the pictures and in the plots. The plots background colors are used to guide the eyes. The filled area in dark blue represents the standard deviations of the chemiluminescence intensity. (For interpretation of the references to color in this figure legend, the reader is referred to the web version of this article.)

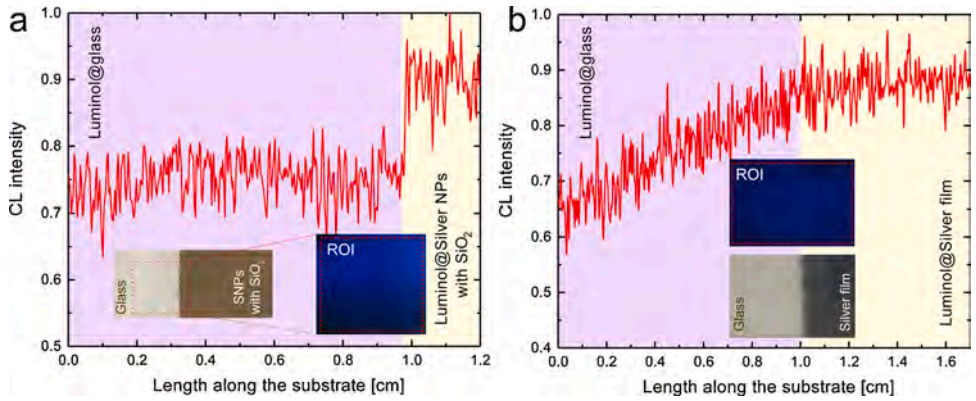


**Fig. 6.** Distribution of chemiluminescence intensities over the indicated ROI for luminol on the dedicated silver metasurface covered by a 2 nm thick $SiO_2$ spacer (a) and on the silver film that have plasmon resonances detuned from the chemiluminescence bands of luminol (b). The insets show also the images of the substrates before the luminol addition.

substrate just at the edge of AgNPs (as shown in the inset of Fig. 4). Then, 30 µl of "*solution 2*" was dripped onto another glass slide and both slides are pressed to each other in such a way that both solutions are mixed. The thickness of the gap between two substrates was estimated as about 10 µm based on the simulation of the oscillations in the transmission spectrum [41]. Then, we took images of the substrates with nanoparticles at the moment of luminol and DPA glowing. The normalized distribution of the CL intensities are demonstrated in Fig. 5a for luminol and Fig. 5b for DPA. The sharp jump in the chemiluminescence intensity of both luminol and DPA is clearly seen at the edges of AgNPs covered regions (Fig. 5). In this respect, we observed that the chemiluminescence intensity of luminol with the presence of AgNPs is enhanced by 1.6 times, while in case of DPA the enhancement factor reaches 1.5.

### 3.2. Influence of the Purcell effect on the MEC

When reagents are contacted directly to the silver metasurface with the plasmon resonances absorption band within the chemiluminescence bands of luminol, the chemiluminescence intensity is increased by 1.6 times. To clarify the relative role of the Purcell effect and the catalytic effect of silver in this enhancement, additional experiments were performed. First, an identical AgNPs substrate was covered with 2 nm $SiO_2$ spacer layer (the inset of Fig. 6a). It was expected that the catalytic effect of AgNPs completely disappears, since it requires direct contact between the reactants and nanoparticles. Nevertheless, in spite of the increased distance between the reactants and AgNPs, the Purcell effect remains. Indeed, in the presence of the spacer, the enhancement factor drops to 1.3 factor (Fig. 6a). It should also be noted that inhomogeneous distribution of the chemiluminescent intensity in the $SiO_2$ area that can be seen in Fig. 6a is due to the tolerances of the applied pressure on microscope cover slip that leads to the slightly uneven distribution of the mixture. Yet, the jump of chemiluminescence intensity at the boundary of the metasurface is clearly visible. Thus, the decisive role of the Purcell effect was confirmed. In this case, an increase in chemiluminescence enhancement with a decrease in the distance between reagents and AgNPs was naturally explained.

In order to estimate the role of catalysis in chemiluminescence enhancement in the absence of the spacer, we also conducted the experiment with a silver film that has no plasmon resonances in the chemiluminescence bands of luminol. If chemiluminescence is also enhanced, this enhancement should be attributed to the catalytic effect of silver. However, in Fig. 6b one can observe no difference in the chemiluminescence intensities from the regions of the plain dielectric substrate and silver film without plasmon resonances. Consequently, the 1.6-fold enhancement of chemiluminescence observed upon direct contact of the reagents with the silver film with plasmon resonances in the chemiluminescence bands is explained by the dominant contribution

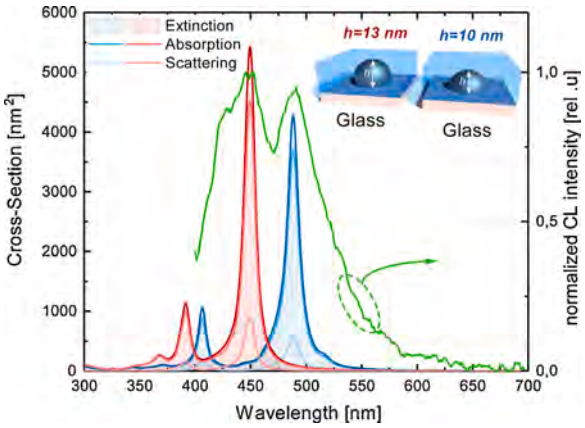


**Fig. 7.** The overlap between the normalized chemiluminescence intensity spectra of luminol solution (green line) and the calculated extinction spectra of AgNPs supported on different substrates and submerged into luminol solution. Extinction cross-section spectra of AgNPs with $h = 13$ nm for the enhancement of luminol chemiluminescence emission band at 452 nm and with $h = 10$ nm for the luminol band at 489 nm. The diameters of AgNPs in both cases are 20 nm. The 3D models of silver nanoparticles placed on the respective substrates and submerged into the luminol solution are illustrated in the inserts. The arrow on the green curve points towards of the corresponding axis. (For interpretation of the references to color in this figure legend, the reader is referred to the web version of this article.)

of the Purcell electrodynamic effect rather than the chemical catalytic effect.

### 3.3. Numerical studies for AgNP@luminol configuration

As shown in Fig. 7, the main luminol chemiluminescence emission bands appear at 452 nm and 489 nm, respectively, while the plasmon resonances of small silver and gold nanospheres in aqueous environment have their maxima at the wavelengths of 415 nm and 528 nm respectively [1]. Hence, the most promising way to establish the desired resonance interaction is to choose silver as the nanoparticles material, and change its (1) size, (2) shape and (3) surrounding. These three approaches may be employed to shift the localized surface plasmons in AgNPs to longer wavelengths. Thus, the dedicated plasmonic-chemiluminophore system design, which benefits from plasmonic nanoparticles tuning, can efficiently enhance the chemiluminescence effect. By taking advantage of the fabrication of AgNPs on dielectric substrates using PVD in ultrahigh vacuum, the long-wavelength shift of the plasmon bands of AgNPs can be achieved

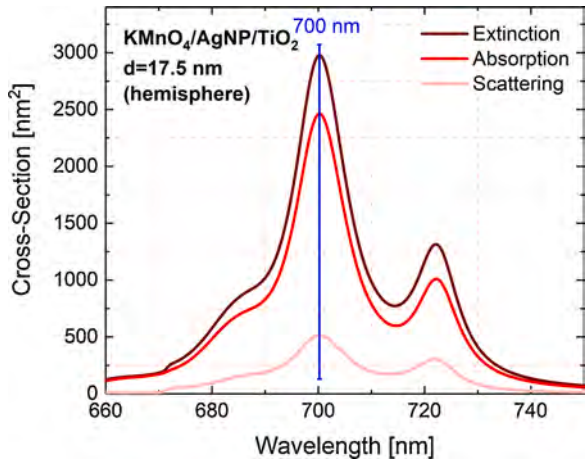


**Fig. 8.** Calculated absorption, scattering and extinction cross-section spectra of the silver nanoparticles deposited on the $TiO_2$ substrate. The diameter of the hemisphere is $d = 17.5$ nm.

by: direct contact of the metal nanoparticles with a substrate having a higher dielectric permittivity than water, as well as the oblated shape of the nanoparticles obtained on surface of the substrate during the deposition process. To explore if these two mechanisms may be well-balanced to provide the desired conditions for the plasmon band, we considered common transparent dielectric substrates: glass, quartz ($SiO_2$), sapphire ($Al_2O_3$), magnesium fluoride ($MgF_2$), and titanium dioxide ($TiO_2$).

Fig. 7 shows extinction, absorption and scattering cross-sections spectra computed for nanoparticles supported on the glass substrate. The supported AgNPs were assumed to be submerged in a luminol solution. Since luminol expected to be diluted with a high ratio in water, the refractive index of the surrounded media was set to that of water, 1.33. The shape of nanoparticles obtained by PVD was assumed to be a hemisphere while their diameter was continuously changed to match the absorption plasmon band to the chemiluminescent emission spectra of luminol. We found out that the absorption cross-section of the optimally-tuned AgNPs is 12 times larger than the geometrical cross-section of AgNPs. According to our calculations presented in Fig. 7, an ideal matching with the first luminol emission peak at 489 nm is achieved for silver hemispheres with 20 nm diameter deposited on the glass substrate (refractive index $n = 1.51$).

However, the calculations show that the absorption plasmon band of AgNPs on the glass substrate provides no spectral overlap with the second luminol chemiluminescence emission peak located at 452 nm even using the smallest hemispheres nanoparticles. Yet, the resonance condition between the absorption plasmon band and the luminol emission peak at 452 nm may be restored for the truncated sphere of 20 nm in diameter and the height of $h = 13$ nm. The possibility for resonance plasmon band tuning of gold nanoparticles toward long-wavelength range has been numerically demonstrated by means of the truncating the spherical nanoparticles [42]. We noticed that the high refractive index substrates (e.g. sapphire having the refractive index as high as 1.77 [43,44] and titanium dioxide substrate) lead to inefficient overlapping of silver absorption plasmon band with the luminol emission since the long-wavelength shift is too large even for the very small silver hemispheres. On the contrary, the high refractive index substrates can be considered for those chemiluminophore molecules that have an emission band in long-wavelength side. Therefore, we assume that to enhance the chemiluminescence effect of luminol using the AgNPs array, the glass substrate is a more reasonable choice.

### *3.4. Numerical calculation for alternative metal-enhanced chemiluminescence configuration on dielectric substrate*

As luminol is not the sole substance that is widely used in various applications as chemiluminophore, here we present a manifold of substrate-nanoparticle pairs optimized for surface-enhanced chemiluminescence. We considered well-known chemiluminophores: $KMnO_4$ in Fig. 8, Lucigenin in Fig. 9a, b, Ce (IV) in Fig. 9c,d, and bis-(2,4,6-tricholorophenyl) oxalate (TCPO) in Fig. 9e,f. We optimized the diameters of silver hemispheres for $KMnO_4$ chemiluminescent emission spectra (Fig. 8) with the emission band maximum at 700 nm [45]. As an alternative example of a chemiluminescent agent, we considered Lucigenin. This substance is widely used in analytical science whereas its the emission band maximum is located at 480 nm [46–49] (Fig. 9a, b). The absorption, scattering and extinction cross-section spectra of silver hemisphere optimized for Cerium (IV) chemiluminescent emission spectra are presented in Fig. 9c, d. The emission band maximum peak lies at ~550 nm [50,51]. Then, we calculated suitable parameters for the plasmon nanoparticle on the top of dielectric substrate for TCPO chemiluminescence emission spectra. The emission band maximum is at 485 nm (Fig. 9e,f) [52].

## 4. Conclusions

In summary, we have proposed a novel approach to designing new materials assembled from nanoparticles for enhancing chemiluminescence, as well as spasing for emerging applications such as DNA profiling and forensic studies. All of them are promising in terms of delivering substantial enhancement in specific and accurate detection of analytes, which is impossible via traditional approaches. We used the proposed technique to fabricate the supported silver nanoparticles ensemble with the plasmon band that peaks at 482 nm and overlaps well with the luminol emission bands. Laser treatment is shown to provide the enhanced chemical and mechanical stability of the obtained thin films materials. Combining these materials with recent advances in the chemiluminescence microfluidic systems opens the door for new chemiluminophores-based light sources. These light sources, where the poor quantum emitter (chemiluminophore) is replaced by high quantum efficiency of plasmonic nanoparticles, could not be achieved by conventional manufacturing processes, in which particles size and shape are fixed. We found that the particle arrangement on the surface of the transparent dielectrics makes it possible to control the distance between the light-emitting species and nanoantennas to elucidate the Purcell effect role in the observed chemiluminescent enhancement. The inert layer, placed on the top of the self-organised metasurface of AgNPs, allows us to eliminate the contribution of catalytic effect in the MEC activity and shows a gain in the luminescence intensity of chemiluminophore molecules due to the retained Purcell effect. We conclude that the fabrication of AgNPs using the physical vapor deposition technique in vacuum, followed by the self-organization of nanoparticles, is an affordable and convenient method leading to plasmonic enhancement for the luminol and *9,10*-diphenylanthracene chemiluminescence.

## Authors' contributions

**Daler R. Dadadzhanova**: Writing – Original draft preparation, Investigation, Writing – Review & Editing, Visualization, Resources.
**Igor A. Gladskikh**: Resources, Investigation.
**Mikhail A. Baranov**: Resources.
**Tigran A. Vartanyan**: Supervision, Writing – Review & Editing.
**Alina Karabchevsky**: Supervision, Writing – Review & Editing.

## Declaration of Competing Interest

The authors report no declarations of interest.

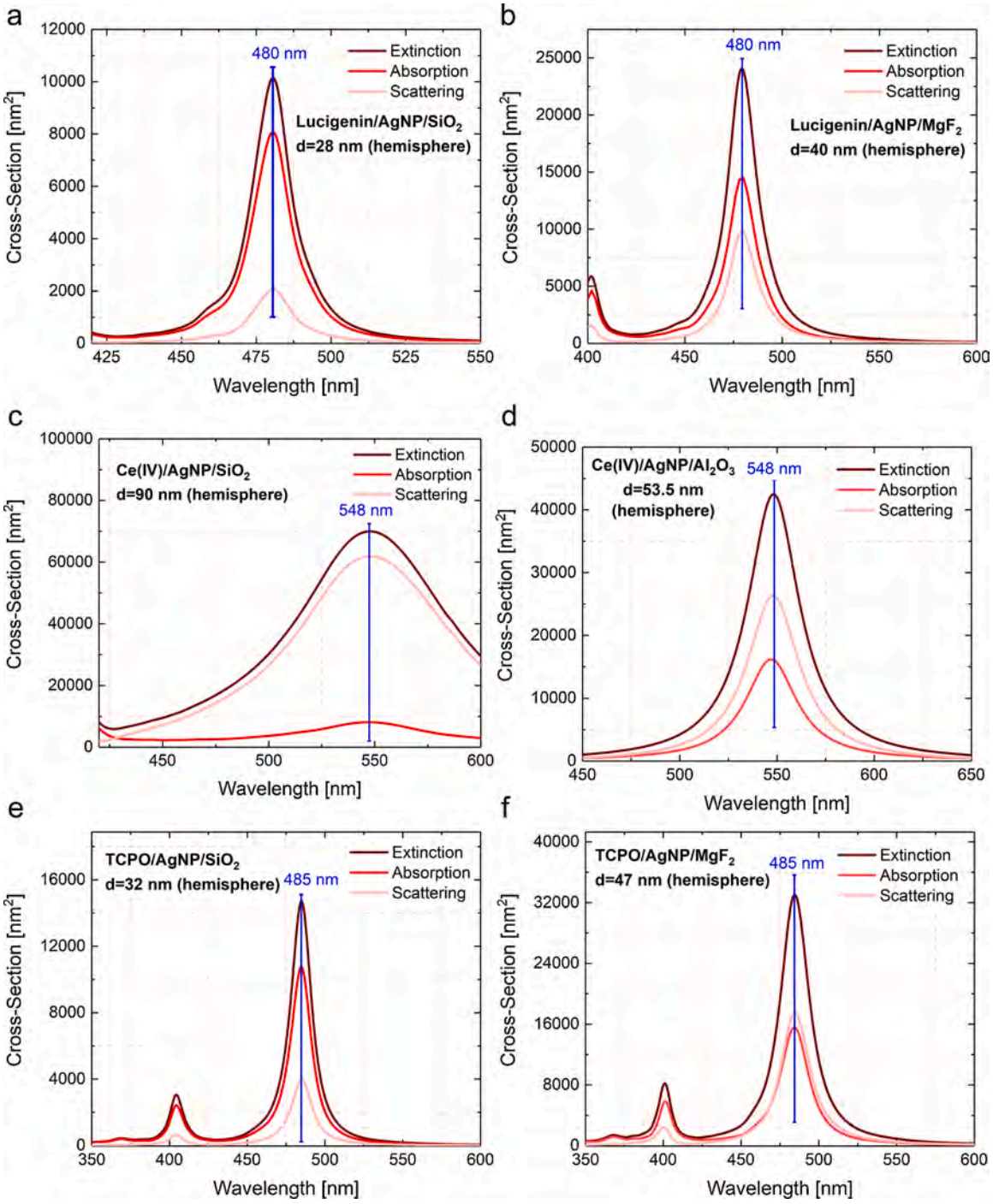


**Fig. 9.** Calculated absorption, scattering and extinction cross-section spectra of the silver nanoparticle: (a) deposited on the $SiO_2$ substrate for Lucigenin. The diameter of the hemisphere is $d = 28$ nm. (b) The silver nanoparticle on the $MgF_2$ substrate with diameter of 40 nm for Lucigenin system; (c) deposited on the $SiO_2$ substrate for Ce (IV). The diameter of the hemisphere is $d = 90$ nm. (d) the silver nanoparticle on the $Al_2O_3$ substrate ($d = 53.5$ nm); (e) deposited on the $SiO_2$ substrate for TCPO system. The diameter of the hemisphere is 32 nm. (f) the silver nanoparticle on the $MgF_2$ substrate with diameter of 47 nm for overlapping with TCPO chemiluminophore.

## Acknowledgement

This work was funded by Israel Science foundation (ISF),No. 2598/20. T.A.V. acknowledges the financial support of Government of Russian Federation,Grant 08-08. The research was performed as part of joint Ph. D. program between the BGU and ITMO. Special thanks to Farrukh Safin for his help with images.

## Appendix A. Supplementary data

Supplementary data associated with this article can be found, in the online version, at https://doi.org/10.1016/j.snb.2021.129453.

## References

[1] A. Karabchevsky, A. Mosayyebi, A.V. Kavokin, Tuning the chemiluminescence of a luminol flow using plasmonic nanoparticles, Light: Sci. Appl. 5 (11) (2016) e16164. ISSN 2047-7538.

[2] F. Barni, S.W. Lewis, A. Berti, G.M. Miskelly, G. Lago, Forensic application of the luminol reaction as a presumptive test for latent blood detection, Talanta 72 (3) (2007) 896–913. ISSN 0039-9140.
[3] S. Yamashoji, Determination of viable mammalian cells by luminol chemiluminescence using microperoxidase, Anal. Biochem. 386 (1) (2009) 119–120. ISSN 0003-2697.
[4] M. Iranifam, Chemiluminescence reactions enhanced by silver nanoparticles and silver alloy nanoparticles: applications in analytical chemistry, TrAC Trends Anal. Chem. 82 (2016) 126–142. ISSN 0165-9936.
[5] R. Freeman, X. Liu, I. Willner, Chemiluminescent and chemiluminescence resonance energy transfer (CRET) detection of DNA, metal ions, and aptamer-substrate complexes using hemin/G-quadruplexes and CdSe/ZnS quantum dots, J. Am. Chem. Soc. 133 (30) (2011) 11597–11604. ISSN 0002-7863.
[6] L.L. Klopf, T.A. Nieman, Effect of iron (II), cobalt (II), copper (II), and manganese (II) on the chemiluminescence of luminol in the absence of hydrogen peroxide, Anal. Chem. 55 (7) (1983) 1080–1083. ISSN 0003-2700.
[7] J. Lee, H.H. Seliger, Quantum yields of the luminol chemiluminescence reaction in aqueous and aprotic solvents, Photochem. Photobiol. 15 (2) (1972) 227–237. ISSN 0031-8655.
[8] R. Fobel, A.E. Kirby, A.H.C. Ng, R.R. Farnood, A.R. Wheeler, Paper microfluidics goes digital, Adv. Mater. 26 (18) (2014) 2838–2843. ISSN 0935-9648.
[9] M.G. Ou, G.W. Lu, H. Shen, A. Descamps, C.A. Marquette, L.J. Blum, G. Ledoux, S. Roux, O. Tillement, B.L. Cheng, Catalytic performance of nanoscale-corrugated gold and silver films for surface-enhanced chemiluminescence, Adv. Funct. Mater. 17 (12) (2007) 1903–1909. ISSN 1616-301X.
[10] A. Karabchevsky, O. Krasnykov, M. Auslender, B. Hadad, A. Goldner, I. Abdulhalim, Theoretical and experimental investigation of enhanced transmission through periodic metal nanoslits for sensing in water environment, Plasmonics 4 (4) (2009) 281. ISSN 1557-1955.
[11] A. Karabchevsky, M. Auslender, I. Abdulhalim, Dual-surface plasmon excitation with thin metallic nanoslits, J. Nanophotonics 5 (1) (2011) 51821. ISSN 1934-2608.
[12] K. Aslan, C.D. Geddes, Metal-enhanced chemiluminescence: advanced chemiluminescence concepts for the 21st century, Chem. Soc. Rev. 38 (9) (2009) 2556–2564.
[13] A. Karabchevsky, I. Abdulhalim, C. Khare, B. Rauschenbach, Microspot sensing based on surface-enhanced fluorescence from nanosculptured thin films, J. Nanophotonics 6 (1) (2012) 61508. ISSN 1934-2608.
[14] I. Abdulhalim, A. Karabchevsky, C. Patzig, B. Rauschenbach, B. Fuhrmann, E. Eltzov, R. Marks, J. Xu, F. Zhang, A. Lakhtakia, Surface-enhanced fluorescence from metal sculptured thin films with application to biosensing in water, Appl. Phys. Lett. 94 (6) (2009) 63106. ISSN 0003-6951.
[15] E.M. Hicks, S. Zou, E.M. Hicks, S. Zou, G.C. Schatz, K.G. Spears, R.P. Van Duyne, L. Gunnarsson, T. Rindzevicius, B. Kasemo, M. Käll, Nano Lett. 5 (2005) 1065.
[16] K. Aslan, C.D. Geddes, Surface plasmon coupled chemiluminescence from zinc substrates: directional chemiluminescence, Appl. Phys. Lett. 94 (7) (2009) 73104. ISSN 0003-6951.
[17] J.-E. Park, J. Kim, J.-M. Nam, Emerging plasmonic nanostructures for controlling and enhancing photoluminescence, Chem. Sci. 8 (7) (2017) 4696–4704.
[18] T.H. Fereja, A. Hymete, T. Gunasekaran, A recent review on chemiluminescence reaction, principle and application on pharmaceutical analysis, ISRN Spectrosc. 2013 (2013).
[19] C.D. Geddes, Surface Plasmon Enhanced, Coupled and Controlled Fluorescence, John Wiley & Sons, 2017. ISBN 1118027930.
[20] L. Wei, Z. Zhujun, Y. Liu, Chemiluminescence microfluidic chip fabricated in PMMA for determination of benzoyl peroxide in flour, Food Chem. 95 (4) (2006) 693–698. ISSN 0308-8146.
[21] A.R. Perestrelo, A.C.P. Águas, A. Rainer, G. Forte, Microfluidic organ/body-on-a-chip devices at the convergence of biology and microengineering, Sensors 15 (12) (2015) 31142–31170.
[22] P.M. Valencia, O.C. Farokhzad, R. Karnik, R. Langer, Microfluidic technologies for accelerating the clinical translation of nanoparticles, Nat. Nanotechnol. 7 (10) (2012) 623. ISSN 1748-3395.
[23] A.U. Rehman Aziz, C. Geng, M. Fu, X. Yu, K. Qin, B. Liu, The role of microfluidics for organ on chip simulations, Bioengineering 4 (2) (2017) 39.
[24] I.M. Lazar, P. Trisiripisal, H.A. Sarvaiya, Microfluidic liquid chromatography system for proteomic applications and biomarker screening, Anal. Chem. 78 (15) (2006) 5513–5524. ISSN 0003-2700.
[25] J. Yu, J. Zhou, A. Sutherland, W. Wei, Y.S. Shin, M. Xue, J.R. Heath, Microfluidics-based single-cell functional proteomics for fundamental and applied biomedical applications, Annu. Rev. Anal. Chem. 7 (2014) 275–295. ISSN 1936-1327.
[26] A. Valero, J. Nicole Post, J.W. van Nieuwkasteele, P.M. ter Braak, W. Kruijer, A. van den Berg, Gene transfer and protein dynamics in stem cells using single cell electroporation in a microfluidic device, Lab Chip 8 (1) (2008) 62–67.
[27] M.R. Bennett, J. Hasty, Microfluidic devices for measuring gene network dynamics in single cells, Nat. Rev. Genet. 10 (9) (2009) 628. ISSN 1471-0064.
[28] N.A. Toropov, I.A. Gladskikh, P.S. Parfenov, T.A. Vartanyan, Fabrication and laser-assisted modification of the Ag particles ensembles supporting quadrupole plasmon oscillations, Opt. Quantum Electron. 49 (4) (2017) 154. ISSN 0306-8919.
[29] N.B. Leonov, I.A. Gladskikh, V.A. Polishchuk, T.A. Vartanyan, Evolution of the optical properties and morphology of thin metal films during growth and annealing, Optics Spectrosc. 119 (3) (2015) 450–455. ISSN 0030-400X.
[30] N. Toropov, T. Vartanyan, Noble metal nanoparticles: synthesis and optical properties, in: D.L. Andrews, R.H. Lipson, T. Nann (Eds.), Comprehensive Nanoscience and Nanotechnology (Second Edition), second edition, Academic Press, Oxford, 2019, pp. 61–88. ISBN 978-0-12-812296-9.
[31] M. Weisenberg, Y. Zhang, C.D. Geddes, Metal-enhanced chemiluminescence from chromium, copper, nickel, and zinc nanodeposits: evidence for a second enhancement mechanism in metal-enhanced fluorescence, Appl. Phys. Lett. 97 (13) (2010) 133103.
[32] M.H. Chowdhury, K. Aslan, S.N. Malyn, J.R. Lakowicz, C.D. Geddes, Metal-enhanced chemiluminescence: radiating plasmons generated from chemically induced electronic excited states, Appl. Phys. Lett. 88 (17) (2006) 173104.
[33] M.H. Chowdhury, S.N. Malyn, K. Aslan, J.R. Lakowicz, C.D. Geddes, Multicolor directional surface plasmon-coupled chemiluminescence, J. Phys. Chem. B 110 (45) (2006) 22644–22651.
[34] F. Jiang, P. Li, C. Zong, H. Yang, Surface-plasmon-coupled chemiluminescence amplification of silver nanoparticles modified immunosensor for high-throughput ultrasensitive detection of multiple mycotoxins, Anal. Chim. Acta (2020).
[35] T.A. Vartanyan, N.B. Leonov, V.V. Khromov, S.G. Przhibelskii, N.A. Toropov, E. N. Kaliteevskaya, Granular metal films on the surfaces of transparent dielectric materials studied and modified via optical means, in: Photonics and Micro-and Nano-structured Materials 2011, vol. 8414, International Society for Optics and Photonics, 2012, p. 841404.
[36] N. Toropov, A. Kamalieva, A. Starovoytov, S. Zaki, T. Vartanyan, Polarized stimulated emission of 2d ensembles of plasmonic nanolasers, Adv. Photonics Res. (2020) 2000083.
[37] N.A. Toropov, A.N. Kamalieva, R.O. Volkov, E.P. Kolesova, D.-O.A. Volgina, S. A. Cherevkov, A. Dubavik, T.A. Vartanyan, Direct enhancement of luminescence of $Cd^{x}Zn^{1-x}Se^{y}S^{1-y}ZnS$ nanocrystals with gradient chemical composition by plasmonic nanoantennas, Optics Laser Technol. 121 (2020) 105821.
[38] D.R. Dadadzhanov, T.A. Vartanyan, A. Karabchevsky, Differential extinction of vibrational molecular overtone transitions with gold nanorods and its role in surface enhanced near-ir absorption (senira), Optics Express 27 (21) (2019) 29471–29478.
[39] J. Bosbach, C. Hendrich, F. Stietz, T. Vartanyan, F. Träger, Ultrafast dephasing of surface plasmon excitation in silver nanoparticles: influence of particle size, shape, and chemical surrounding, Phys. Rev. Lett. 89 (25) (2002) 257404.
[40] P.B. Johnson, R.-W. Christy, Optical constants of the noble metals, Phys. Rev. B 6 (12) (1972) 4370.
[41] J.C. Manifacier, J. Gasiot, J.P. Fillard, A simple method for the determination of the optical constants n, k and the thickness of a weakly absorbing thin film, J. Phys. E: Sci. Instrum. 9 (11) (1976) 1002.
[42] V. Devaraj, H. Jeong, C. Kim, J.-M. Lee, J.-W. Oh, Modifying plasmonic-field enhancement and resonance characteristics of spherical nanoparticles on metallic film: effects of faceting spherical nanoparticle morphology, Coatings 9 (6) (2019) 387.
[43] M.W. Knight, Y. Wu, J. Britt Lassiter, P. Nordlander, N.J. Halas, Substrates matter: influence of an adjacent dielectric on an individual plasmonic nanoparticle, Nano Lett. 9 (5) (2009) 2188–2192. ISSN 1530-6984.
[44] X. Liu, D. Li, X. Sun, Z. Li, H. Song, H. Jiang, Y. Chen, Tunable dipole surface plasmon resonances of silver nanoparticles by cladding dielectric layers, Sci. Rep. 5 (2015) 12555. ISSN 2045-2322.
[45] C.M. Hindson, P.S. Francis, G.R. Hanson, J.L. Adcock, N.W. Barnett, Mechanism of permanganate chemiluminescence, Anal. Chem. 82 (10) (2010) 4174–4180. ISSN 0003-2700.
[46] Y. He, H. Cui, Fabrication of luminol and lucigenin bifunctionalized gold nnanoparticles/graphene oxide nanocomposites with dual-wavelength chemiluminescence, J. Phys. Chem. C 116 (23) (2012) 12953–12957. ISSN 1932-7447.
[47] J.-Z. Guo, H. Cui, Lucigenin chemiluminescence induced by noble metal nanoparticles in the presence of adsorbates, J. Phys. Chem. C 111 (33) (2007) 12254–12259. ISSN 1932-7447.
[48] T. Okajima, T. Ohsaka, Chemiluminescence of lucigenin by electrogenerated superoxide ions in aqueous solutions, Luminescence 18 (1) (2003) 49–57. ISSN 1522-7235.
[49] B. Liu, Y. He, C. Duan, N. Li, H. Cui, Platinum nanoparticle-catalyzed lucigenin-hydrazine chemiluminescence, J. Photochem. Photobiol. A: Chem. 217 (1) (2011) 62–67. ISSN 1010-6030.
[50] X. Yu, Q. Wang, X. Liu, X. Luo, A sensitive chemiluminescence method for the determination of cysteine based on silver nanoclusters, Microchim. Acta 179 (3–4) (2012) 323–328. ISSN 0026-3672.
[51] S.-F. Li, X.-M. Zhang, Z.-J. Yao, R. Yu, F. Huang, X.-W. Wei, Enhanced chemiluminescence of the rhodamine 6G-cerium (IV) system by Au- Ag alloy nanoparticles, J. Phys. Chem. C 113 (35) (2009) 15586–15592. ISSN 1932-7447.
[52] L. Wang, Y. Tang, Determination of dipyridamole using TCPO-H2O2 chemiluminescence in the presence of silver nanoparticles, Luminescence 26 (6) (2011) 703–709. ISSN 1522-7235.
[53] M. Mirasoli, M. Guardigli, A. Roda, Chemiluminescence in biomedicine. Applied Photochemistry, Springer, 2016, pp. 427–458.

**Daler Dadadzhanov** obtained his double MSc degree in Physics in Aalto University Finland and ITMO University Russian Federation in 2016. From 2017 he is a member of the Light-on-a-Chip group at Electrooptics and Photonics Department at School of Electrical and Computer Engineering at Ben-Gurion University of the Negev (BGU) as a Ph.D. student jointly supervised by Dr. Alina Karabchevsky (BGU, Israel) and Dr. Tigran A. Vartanyan (ITMO, St Petersburg, Russian Federation). He is interested in integrated photonics, plasmonics and sensing.

**Dr. Igor Gladskikh** is Ph.D., researcher of Center for Information Optical Technologies. His scientific interest is in the production of metal nanostructures, their processing and

characterization. Mikhail Baranov obtained his MSc from ITMO University. He is interested in electron microscopy (SEM, TEM, STEM), EDX, WDX, crystallography mapping, nanoscale optics.

**Dr. Tigran A. Vartanyan** is a Head of Laboratory for Surface Photophysics of the Center of Information Optical Technologies at ITMO University, St. Petersburg, Russia. His research interests are in nanoplasmonics, nonlinear optics, spectroscopy, and atomic and molecular collisions. He serves as the deputy Editor-in-Chief of the international journal Optics and Spectroscopy published by Springer Nature, and the Editorial Board member of the Journal of Optical Technology published by the Optical Society of America.

**Dr. Alina Karabchevsky** is a Senior Lecturer (Assistant Professor) at the Department of Electrooptics and Photonics Engineering of School of Electrical and Computer Engineering at Ben-Gurion University of the Negev. She is an expert in integrated photonics, biophotonics, plasmonics and microfluidics. Dr. Alina Karabchevsky received her PhD in 2013 and was awarded with 'Outstanding Woman in Science' President's award. From 2013 to 2015 she was affiliated with the Southampton University as a postdoc and further as a Research Assistant. In 2014 she was awarded with Brilliance in research prize by the Director of Optoelectronics Research Centre Prof Sir Dave Payne. From 2015, Dr. Karabchevsky is affiliated with Ben-Gurion University in which she established and leading the State-of-Art integrated Photonics laboratory in Israel named Light-on-a-Chip group.